www.sciencemag.org/cgi/content/full/science.aaq0186/DC1

Supplementary Materials for

Early spectra of the gravitational wave source GW170817: Evolution of a neutron star merger

B. J. Shappee,* J. D. Simon, M. R. Drout, A. L. Piro, N. Morrell, J. L. Prieto, D. Kasen, T. W.-S. Holoien, J. A. Kollmeier, D. D. Kelson, D. A. Coulter, R. J. Foley, C. D. Kilpatrick, M. R. Siebert, B. F. Madore, A. Murguia-Berthier, Y.-C. Pan, J. X. Prochaska, E. Ramirez-Ruiz, A. Rest, C. Adams, K. Alatalo, E. Bañados, J. Baughman, R. A. Bernstein, T. Bitsakis, K. Boutsia, J. R. Bravo, F. Di Mille, C. R. Higgs, A. P. Ji, G. Maravelias, J. L. Marshall, V. M. Placco, G. Prieto, Z. Wan

*Corresponding author. Email: shappee@hawaii.edu

Published 16 October 2017 on *Science* First Release
DOI: 10.1126/science.aaq0186

This PDF file includes:

Materials and Methods

S1 Data Acquisition & Reductions

We obtained spectroscopic observations of SSS17a with the Magellan/Clay and Magellan/Baade telescopes beginning 11.75 hours after the neutron star merger, and continued observing SSS17a spectroscopically for 8 days. Below we describe the data acquisition, reduction, and calibration. A log of all spectroscopic observations is given in Table S1.

S1.1 LDSS-3 Observations

We observed SSS17a with the Low Dispersion Survey Spectrograph (LDSS-3) on the Magellan/Clay telescope on 2017 Aug. 18-26 (UT). On the first night we obtained spectra in multiple spectrograph configurations, with the Volume Phase Holographic (VPH)-All, VPH-Blue, and VPH-Red grisms. The three grisms cover wavelength ranges of $3800-6200$ Å, $4250-10000$ Å, and $6000-10000$ Å with resolving powers of $R = 1400$, $R = 650$, and $R = 1400$, respectively. The later LDSS-3 spectroscopy, when SSS17a was much fainter and redder, employed only the VPH-All or VPH-Red grisms. All observations were made with a slit width of 1 arcsec.

We reduced and calibrated the LDSS-3 spectra using IRAF (*47*) following standard procedures, including bias subtraction, flat-fielding, 1-D spectral extraction, and wavelength calibration by comparison to an arc lamp. Flux calibration and telluric correction was performed using a set of custom IDL scripts (*48,49*) based on a spectroscopic standard star observed on the same night. The statistical uncertainties on the spectra were calculated by standard error propagation.

For the first LDSS-3 spectra of SSS17a, obtained on 2017 Aug. 17-18, the spectrograph slit was oriented $\sim 22^{\circ}$ away from parallactic angle. Given the relatively high airmass ($\mathrm{airmass} \approx 2$) at the time, some flux was lost as a result of differential atmospheric refraction. A similar offset from parallactic angle was used for LDSS-3 observations on 2017 Aug. 18-19, with

smaller flux losses because of the lower airmass. To correct for this effect, we first calculated the offset of the source from the center of the slit due to the differential refraction, assuming that the target was in the center of the slit at the effective central wavelength of the g filter that was used for target acquisition. We then measured the atmospheric seeing as a function of wavelength, modeled the source with a two-dimensional Gaussian profile, and computed the fraction of light from the model source that fell in the slit as a function of wavelength. Finally, the calibrated spectrum of SSS17a was scaled to account for the light that landed outside the slit.

The magnitude of the differential refraction and seeing corrections depends on the position of the source within the slit. A source position different than the one we have assumed will result in systematic errors in the scaled spectrum. Because we do not have a way of measuring this position during the spectroscopic exposure, we quantify the resulting systematic uncertainty by calculating the change in the differential refraction and seeing corrections for source positions offset by 0.1 arcsec in either direction (over a 300 s exposure the telescope guiding is expected to be at least this accurate) from the nominal position. At each wavelength, we define the systematic uncertainty to be the average of the changes in the correction factor between the $+0.1$ arcsec and -0.1 arcsec offsets.

S1.2 MagE Observations

We observed SSS17a with the Magellan/MagE spectrograph (*50*) on the nights of 2017 August 17-19. We used a $0.7 \text{ arcsec} \times 10 \text{ arcsec}$ slit to provide a spectral resolving power of $R = 5800$ on August 17-18 and a $1.0 \text{ arcsec} \times 10 \text{ arcsec}$ slit to provide a spectral resolving power of $R = 4100$ on August 18-19. On the first night we obtained a single 322 s exposure and on the second night we obtained three 1000 s exposures. We reduced the MagE spectra using an IDL pipeline based on the techniques described in (*51*), with updates to improve the flux calibration

from (*52*). Observations on both nights were flux calibrated with a standard star spectrum obtained on 2017 Aug. 18-19.

The spectrum from Aug. 17-18 was taken with the slit oriented at the parallactic angle, so the effects of differential atmospheric refraction should be negligible despite the high airmass (3.0) at the time of observation. The seeing measured from the spatial profile of the source spectrum varied as a function of wavelength, from 0.9 arcsec at the red end of the spectrum to 1.3 arcsec in the blue. We corrected for wavelength-dependent loss of light from this seeing variation by modeling the source with a two-dimensional Gaussian profile, calculating the fraction of the flux that fell in the slit as a function of wavelength, and adjusting the calibrated spectrum accordingly.

For readers who are interested in making use of the Aug. 17-18 MagE spectrum, we urge caution in interpreting the data at wavelengths redder than ~ 7000 Å. As a specific example, the apparent step in the spectrum at ~ 7200 Å is not a real feature. It occurs at the breakpoint between two spectral orders and at a wavelength where there is significant telluric absorption, which makes matching the continuum levels of the neighboring orders difficult.

The Aug. 18-19 spectra were obtained with the slit 22° away from parallactic angle, causing a loss of flux at short wavelengths, which we corrected as described above for LDSS-3.

The statistical uncertainties on the MagE spectra were calculated by standard error propagation. We added these in quadrature with additional uncertainties based on the seeing losses, telluric absorption corrections, and the overlap between adjacent spectral orders. To be conservative we applied generous uncertainties for each of these effects. For wavelengths within 20 Å of where orders overlap we assumed a 30% uncertainty on the measured fluxes. We also assumed that the seeing loss and telluric corrections each had an uncertainty of 30%.

S1.3 IMACS Observations

We observed SSS17a with IMACS (*53*) on the Magellan/Baade telescope approximately 48 hours after its discovery on 2017 Aug. 19-20 using the f/2 camera and the 300 lines/mm grism at a blaze angle of 17.5°. The spectrum was obtained through a 0.9 arcsec-wide slit providing a spectral resolving power of $R \sim 1000$. We reduced and extracted the IMACS spectrum using standard routines in IRAF, including a telluric correction.

S1.4 MIKE Observations

We obtained spectra of SSS17a totaling 1.03 hours of integration time with the MIKE spectrograph (*55*) using a $2 \ \mathrm{arcsec} \times 5 \ \mathrm{arcsec}$ slit beginning at UT 00:18 on 2017 Aug 19. The wide slit ensured that we captured as much light as possible from the fading transient. For light that fills a 2 arcsec slit the resulting resolving power is $R = 13000$ in the red ($\lambda > 5000$ Å) and $R = 16000$ in the blue ($\lambda < 5000$ Å). However, the seeing of ~ 1 arcsec during the observations provides resolving power a factor of ~ 2 higher for the SSS17a spectrum. We reduced these data using the Carnegie Python pipeline (*55*). The spectrum has a signal-to-noise ratio of 8 per pixel at 5900 Å and 12 per pixel at 6600 Å and is shown in Figure S1.

S1.5 Calibrating and Dereddening Spectra of SSS17a

We futher calibrate the non-MIKE spectra (LDSS-3, MagE, and IMACS) against photometric measurements of SSS17a by extracting synthetic photometric magnitudes for each filter that was completely contained in the wavelength range covered by the spectrum and for which we could either interpolate the photometric light curves (*24, 26*) or extrapolate them by no more than 1 hour. The exception is the final (8.46 day) spectrum, where the i band magnitude was linearly extrapolated by 1 day. Then we determined the best-fitting line to the difference between the observed and synthetic photometry as a function of central wavelength, and scaled

each spectrum by this fit. The VPH-blue and VPH-red observations on the first night only covered the wavelengths of g and i, respectively. Thus, for these two spectra we could not correct any wavelength-dependent flux calibration issues and instead only applied a zero-point correction. The bands used to calibrate each spectrum are listed in Table S1.

We adopt reddening and extinction estimates of $E(B{-}V)$ = 0.106 and $A_{\rm V} = 0\ .34$ mag for our analysis based on the far-infrared dust maps of (*56*). These measurements are consistent with the extinction value of $A_{\rm V} = 0\ .37 \pm 0.06$ mag determined by (*57*) using Pan-STARRS1 stellar colors. As a consistency check, we also estimated the extinction along the line of sight to SSS17a with the Na I D absorption lines in the MIKE data. We modeled the Na lines from the Milky Way with a single Gaussian component for each of the D2 and D1 lines, which provides an accurate fit to the spectrum (Figure S1). The spectrum can also be fit with additional weaker components, but because of the modest signal-to-noise ratio of the data and the presence of residuals from the subtraction of the telluric Na D emission lines at nearly the same velocity, those features are not statistically significant. We measured a best-fitting heliocentric velocity of 4.7 ± 1.2 km s^{-1} for this absorbing gas, with a full width at half maximum (FWHM) of 26 ± 3 km s^{-1} and equivalent widths (EWs) of $328{\pm}52$ mÅ for the D2 line and $256{\pm}62$ mÅ for the D1 line. We calculated a Na I column density of 5.2×10^{12} cm^{-2} from the EW measurements using a standard curve-of-growth analysis. This column density corresponds to a V-band extinction $A_{\rm V} \approx 0.4$ mag (*58*). Although this value is consistent with the results of (*56*) and (*57*), because of the uncertainties involved in translating Na D absorption strength into extinction we do not make further use of it in this paper.

We correct the observed spectra for this foreground reddening using a Milky Way extinction curve (*59*). The extinction curve is parameterized by the value $R_V{\equiv}\ A_V/E(B{-}V)$, where $E(B-V) \equiv A_B - A_V$ is the selective extinction between the B and V photometric bands (A_B is the total extinction in the B-band). We assume $R_V = 3.1$.

S1.6 Synthetic Photometry of SSS17a

We measured synthetic photometry in any Sloan ($griz$) or Johnson/Cousins (BVRI) photometric bandpass whose transmission window falls within the wavelength range of the observed spectrum. In order to facilitate direct comparison to broadband observations of SSS17a, this photometry was performed after correction for slit losses, but before the correction for Milky Way reddening described above. To estimate the uncertainties on the synthetic magnitude measurements we run a Monte Carlo simulation. We randomly redraw the photometric measurements 50,000 times based on the observed photometry (*26*), assuming that the photometric uncertainties are normally distributed around the measured magnitudes with a width given by the photometric uncertainties. For each draw, we recalibrate the spectrum to the drawn photometry and then perform synthetic photometry. We adopt the 16th and 84th percentiles of the distribution of synthetic magnitude measurements in the Monte Carlo simulation as the 1σ uncertainties on each measurement. For the day 8.46 spectrum we do not make any synthetic measurements because the photometry used to calibrate that spectrum was extrapolated from one day earlier. We report the synthetic photometry and associated uncertainties in Table S2.

S1.7 GRB130603B Spectra

Both GRB130603B spectra plotted in Figure 2 were presented in (*33*). The GTC/OSIRIS spectrum was taken from that paper while we retrieved and reduced the raw X-Shooter optical and near-infrared spectra using the ESO Reflex environment and the X-Shooter standard pipeline recipes. These spectra are mostly featureless within the noise, except for telluric lines and narrow Mg and Ca absorption.

S2 Constraints on Host Galaxy Absorption Lines

We searched the MIKE and MagE spectra for host galaxy absorption or emission lines. The host galaxy, NGC 4993 (*24*), has a redshift of $z = 0\ .00988$ (*60*). We are unable to detect any absorption lines associated with the host galaxy.This result is in agreement with the results of VLT/X-Shooter observations (*61*). Specifically, we do not detect host galaxy Na D absorption, from which we conclude that all of the extinction along the line of sight to SSS17a is located in the Milky Way. Assuming the same linewidth as for the Milky Way Na D absorption (S1.5) and using the formula given by (*62*), we place a 2σ upper limit on host galaxy Na D absorption of 92 mÅ (for either the D2 or D1 lines). In comparison, the detected Na D EWs for GRB130603B were 530 ± 90 mÅ and 590 ± 80 mÅ for the D2 and D1 lines, respectively (*33*). The signal-to-noise ratio of the MIKE spectrum in the blue is too low to place meaningful constraints on Ca H and K absorption. The lack of any neutral gas in NGC 4993 near the site of the merger might indicate that SSS17a was on the near side of the host galaxy, or that NGC 4993 is a largely gas-free system. We also do not detect Hα in either absorption or emission (with a 2σ upper limit of 63 mÅ for a linewidth of $25\,\mathrm{km\,s^{-1}}$) or the O III $\lambda5007$ Å emission line, although the signal-to-noise ratio of the spectrum near 5000 Å is low because it is close to the wavelength of the dichroic of the spectrograph.

S3 BlackBody Spectral Fitting

We fit blackbody models to the observed dereddened rest-frame spectra from the first night using Markov Chain Monte Carlo (MCMC) methods. For a single MCMC run, the statistical uncertainties described above for the LDSS-3 (S1.1) and MagE (S1.2) spectra define the width of the posterior probability distributions for the blackbody temperatures and radii. We carry out additional Monte Carlo simulations to incorporate the effects of systematic uncertainties

on the spectra and the photometric flux measurements to which they are tied (S1.5). For the LDSS-3 spectrum we draw 500 random positions of the source within the slit from a Gaussian distribution with a FWHM of 0.1 arcsec. We scale the observed spectrum by the slit losses from differential atmospheric refraction and seeing for each of the randomly drawn source positions to create 500 Monte Carlo spectra. We also randomly draw 5 g and i magnitudes for each source position based on the measured photometric uncertainties and scale the Monte Carlo spectra accordingly. We then re-run the MCMC with the resulting spectra. The reported uncertainties on the BB temperatures and radii are the 90% confidence intervals from these 2500 Monte Carlo iterations. Because the MagE spectrum was obtained at parallactic angle there is no systematic component to the spectroscopic uncertainties. The uncertainties related to the photometry still apply, so we randomly draw 2000 g and i magnitudes, scale the spectrum, re-run the MCMC on the Monte Carlo spectra, and define the uncertainties as above.

Figure 1 shows the observed spectra as well as shaded regions with lower and upper bounds corresponding to the blackbody spectra expected for the 5th and 95th percentile temperature and radii obtained from the fits, respectively.

S4 Existing Kilonova Models

There are many theoretical models of kilonovae in the literature, but they have been developed with few observational constraints. To investigate whether any aspects of the SSS17a spectra agree with theoretical predictions, we searched the three main classes of published models: i) classic lanthanide-rich red kilonova (*17*), ii) lanthanide-poor accretion disk winds following the merger (*19*), and iii) a model including both hydrodynamical ejecta and wind from a black hole (BH)-neutron star (NS) merger (*63*). We find that no existing model we considered simultaneously produced satisfactory fits to the spectroscopic features, color, evolution, and luminosity of our spectroscopic time series. However, studying the ways in which models do agree often

leads to additional physical insights. Therefore, we re-examined the models for qualitative similarities with the data by scaling the model luminosities at each epoch to match the observed spectroscopic times series. Even with that additional freedom almost all models were unsatisfactory. However, for the two models shown in Figures 4A and 4B some features resemble the spectra of SSS17a. The NS-NS merger model of (*17*) has 0.1 solar masses of ejecta composed of Ca, Fe, and Nd distributed in a broken power law density profile with $v = 0.2c$. The resulting spectra exhibit smooth red continua with a similar shape to the observed spectra from 4.51 days onward, with the exception of the predicted emission feature at $\sim$ 6000 Å (Figure 4A). Conversely, the disc wind outflow model of (*19*) with a NS with lifetime of 0 ms reproduces the spectral slopes during the first 3.5 days. However, it strongly over-predicts absorption features and under-predicts the photospheric velocity after the merger.

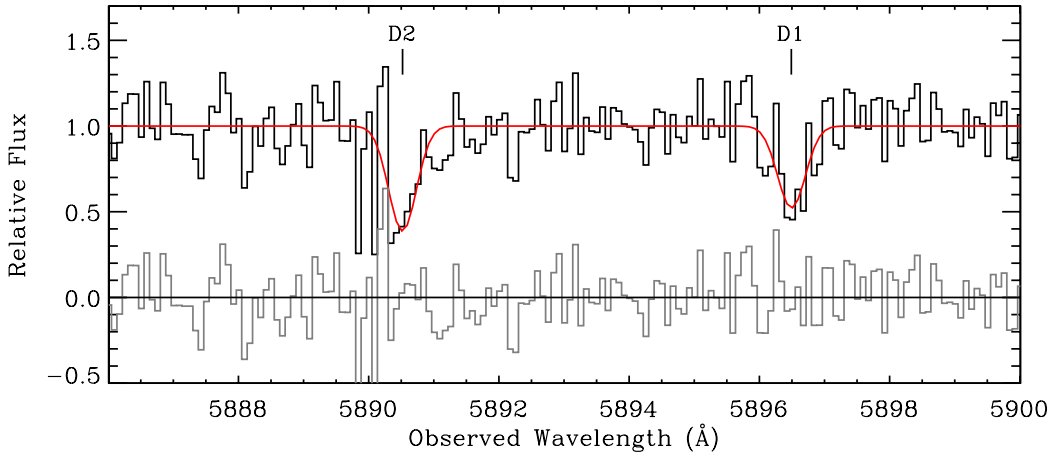

Figure S1. High-resolution MIKE spectrum of SSS17a. The plotted wavelength range is centered on the Na I D absorption lines from the interstellar medium of the Milky Way. The red curve is our Gaussian fit to the spectrum, and the gray spectrum below is the residuals from the fit.

Table S1: **Spectroscopic Observations of SSS17a.** Columns include the UT Date and Julian Date (JD) at the start of the observation, rest frame days since the gravitational wave trigger (phase), the telescope and instrument with which the observations were taken, the rest frame wavelength range of the spectrum, the total exposure time of the spectrum, and the broad-band photometric filters that were used to calibrate the spectrum.

UT Date	JD	phase (days)	Telescope/Instrument	Wavelength range (Å)	Exposure (s)	Calibrating Filters
2017-08-18 00:26:16.9	2457983.518251	0.49	Magellan-Clay/LDSS-3	$3780-10200$	300	g,i
2017-08-18 00:40:08.6	2457983.527877	0.50	Magellan-Clay/LDSS-3	$3800-6200$	300	g
2017-08-18 00:52:08.6	2457983.536204	0.51	Magellan-Clay/LDSS-3	$6450-10000$	600	i
2017-08-18 01:26:22	2457983.559977	0.53	Magellan-Baade/MagE	$3650-10100$	322	g,i
2017-08-18 23:47:36.7	2457984.491397	1.46	Magellan-Clay/LDSS-3	$3820-9120$	600	g,V,r,i
2017-08-19 00:18:11	2457984.512627	1.48	Magellan-Clay/MIKE	$3900-9400$	3710	N/A
2017-08-19 00:35:25	2457984.524595	1.50	Magellan-Baade/MagE	$3800-10300$	3000	g,V,r,i
2017-08-20 00:26:27.9	2457985.518368	2.49	Magellan-Baade/IMACS	$4355-8750$	2100	V,r,i
2017-08-20 23:45:52.7	2457986.490193	3.46	Magellan-Clay/LDSS-3	$4450-10400$	3000	V,r,i,z
2017-08-22 00:50:33.7	2457987.535112	4.51	Magellan-Clay/LDSS-3	$5010-10200$	3600	i,z
2017-08-24 23:33:51.5	2457990.481846	7.45	Magellan-Clay/LDSS-3	$6380-10500$	3600	i,z
2017-08-25 23:39:18.1	2457991.485626	8.46	Magellan-Clay/LDSS-3	$6380-10500$	3600	i^*,z

*This data point was extrapolated from the latest measurement on the previous night.

Table S2: **Synthetic photometry measurements from spectroscopic observations of SSS17a.** Columns include the Julian Date (JD) of the spectroscopic observation and the broadband filter of the measurement ($grizBVR$ or I). Synthetic photometry was performed prior to correction for foreground Milky Way reddening. $griz-$band magnitudes are presented on the AB magnitude scale. $BVRI-$band magnitudes are presented on the Vega magnitude scale. 1σ uncertainties are listed.

JD	g	r	i	z	B	V	R	I
	(AB mag)				(Vega mag)			
2457983.518251	$17.39^{+0.02}_{-0.02}$	$17.33^{+0.02}_{-0.01}$	$17.47^{+0.02}_{-0.02}$	$17.67^{+0.03}_{-0.03}$	...	$17.33^{+0.02}_{-0.02}$	$17.15^{+0.01}_{-0.01}$	$17.08^{+0.02}_{-0.02}$
2457983.527877	$17.41^{+0.02}_{-0.02}$	...	...	...	...	...	...	...
2457983.559977	$17.45^{+0.02}_{-0.02}$	$17.34^{+0.01}_{-0.01}$	$17.51^{+0.02}_{-0.02}$	$17.59^{+0.03}_{-0.02}$	$17.63^{+0.03}_{-0.02}$	$17.35^{+0.02}_{-0.02}$	$17.17^{+0.01}_{-0.01}$	$17.12^{+0.02}_{-0.02}$
2457984.491397	$18.64^{+0.02}_{-0.02}$	$17.92^{+0.01}_{-0.01}$	$17.78^{+0.02}_{-0.02}$	...	...	$18.18^{+0.01}_{-0.01}$	$17.67^{+0.01}_{-0.01}$	$17.31^{+0.03}_{-0.02}$
2457985.518368	...	$18.98^{+0.04}_{-0.05}$	$18.36^{+0.02}_{-0.02}$	...	...	$19.49^{+0.07}_{-0.08}$	$18.57^{+0.03}_{-0.03}$	$17.82^{+0.04}_{-0.04}$
2457986.490193	...	$19.88^{+0.05}_{-0.05}$	$18.91^{+0.04}_{-0.04}$	$18.38^{+0.05}_{-0.05}$	...	$20.41^{+0.08}_{-0.08}$	$19.35^{+0.04}_{-0.04}$	$18.26^{+0.04}_{-0.04}$
2457987.535112	...	$21.00^{+0.14}_{-0.12}$	$19.43^{+0.04}_{-0.04}$	$18.75^{+0.08}_{-0.08}$	...	$21.83^{+0.22}_{-0.17}$	$20.19^{+0.09}_{-0.07}$	$18.67^{+0.04}_{-0.04}$
2457990.481846	...	...	$21.44^{+0.20}_{-0.20}$	$19.91^{+0.07}_{-0.07}$	...	...	...	$20.37^{+0.11}_{-0.10}$

References and Notes

1. B. Paczynski, Gamma-ray bursters at cosmological distances. *Astrophys. J.* **308**, L43 (1986). doi:10.1086/184740

2. D. Eichler, M. Livio, T. Piran, D. N. Schramm, Nucleosynthesis, neutrino bursts and γ-rays from coalescing neutron stars. *Nature* **340**, 126–128 (1989). doi:10.1038/340126a0

3. W. Fong, E. Berger, R. Margutti, B. A. Zauderer, A decade of short-duration gamma-ray burst broadband afterglows: Energetics, circumburst densities, and jet opening angles. *Astrophys. J.* **815**, 102 (2015). doi:10.1088/0004-637X/815/2/102

4. L.-X. Li, B. Paczyński, Transient events from neutron star mergers. *Astrophys. J.* **507**, L59–L62 (1998). doi:10.1086/311680

5. S. R. Kulkarni, Modeling supernova-like explosions associated with gamma-ray bursts with short durations. arXiv:astro-ph/0510256 [astro-ph] (10 October 2005).

6. B. D. Metzger, G. Martínez-Pinedo, S. Darbha, E. Quataert, A. Arcones, D. Kasen, R. Thomas, P. Nugent, I. V. Panov, N. T. Zinner, Electromagnetic counterparts of compact object mergers powered by the radioactive decay of *r*-process nuclei. *Mon. Not. R. Astron. Soc.* **406**, 2650–2662 (2010). doi:10.1111/j.1365-2966.2010.16864.x

7. L. F. Roberts, D. Kasen, W. H. Lee, E. Ramirez-Ruiz, Electromagnetic transients powered by nuclear decay in the tidal tails of coalescing compact binaries. *Astrophys. J.* **736**, L21 (2011). doi:10.1088/2041-8205/736/1/L21

8. B. D. Metzger, Kilonovae. *Living Rev. Relativ.* **20**, 3 (2017). doi:10.1007/s41114-017-0006-z Medline

9. E. M. Burbidge, G. R. Burbidge, W. A. Fowler, F. Hoyle, Synthesis of the elements in stars. *Rev. Mod. Phys.* **29**, 547–650 (1957). doi:10.1103/RevModPhys.29.547

10. A. G. W. Cameron, Nuclear reactions in stars and nucleogenesis. *Publ. Astron. Soc. Pac.* **69**, 201 (1957). doi:10.1086/127051

11. Y.-Z. Qian, G. J. Wasserburg, Where, oh where has the *r*-process gone? *Phys. Rep.* **442**, 237–268 (2007). doi:10.1016/j.physrep.2007.02.006

12. M. Arnould, S. Goriely, K. Takahashi, The *r*-process of stellar nucleosynthesis: Astrophysics and nuclear physics achievements and mysteries. *Phys. Rep.* **450**, 97–213 (2007). doi:10.1016/j.physrep.2007.06.002

13. N. R. Tanvir, A. J. Levan, A. S. Fruchter, J. Hjorth, R. A. Hounsell, K. Wiersema, R. L. Tunnicliffe, A 'kilonova' associated with the short-duration γ-ray burst GRB 130603B. *Nature* **500**, 547–549 (2013). doi:10.1038/nature12505 Medline

14. E. Berger, W. Fong, R. Chornock, An *r*-process kilonova associated with the short-hard GRB 130603B. *Astrophys. J.* **774**, L23 (2013). doi:10.1088/2041-8205/774/2/L23

15. M. M. Kasliwal, O. Korobkin, R. M. Lau, R. Wollaeger, C. L. Fryer, Infrared emission from kilonovae: The case of the nearby short hard burst GRB 160821B. *Astrophys. J.* **843**, L34 (2017). doi:10.3847/2041-8213/aa799d

16. D. Kasen, N. R. Badnell, J. Barnes, Opacities and spectra of the *r*-process ejecta from neutron star mergers. *Astrophys. J.* **774**, 25 (2013). doi:10.1088/0004-637X/774/1/25

17. J. Barnes, D. Kasen, Effect of a high opacity on the light curves of radioactively powered transients from compact object mergers. *Astrophys. J.* **775**, 18 (2013). doi:10.1088/0004-637X/775/1/18

18. M. Tanaka, K. Hotokezaka, Radiative transfer simulations of neutron star merger ejecta. *Astrophys. J.* **775**, 113 (2013). doi:10.1088/0004-637X/775/2/113

19. D. Kasen, R. Fernández, B. D. Metzger, Kilonova light curves from the disc wind outflows of compact object mergers. *Mon. Not. R. Astron. Soc.* **450**, 1777–1786 (2015). doi:10.1093/mnras/stv721

20. LIGO/Virgo collaboration, *GRB Coordinates Network* 21509 (2017).

21. GBM-LIGO, *GRB Coordinates Network* 21506 (2017).

22. INTEGRAL, *GRB Coordinates Network* 21507 (2017).

23. One-Meter Two-Hemisphere (1M2H) collaboration, *GRB Coordinates Network* 21529 (2017).

24. D. A. Coulter, R. J. Foley, C. D. Kilpatrick, M. R. Drout, A. L. Piro, B. J. Shappee, M. R. Siebert, J. D. Simon, N. Ulloa, D. Kasen, B. F. Madore, A. Murguia-Berthier, Y.-C. Pan, J. X. Prochaska, E. Ramirez-Ruiz, A. Rest, C. Rojas-Bravo, Swope Supernova Survey 2017a (SSS17a), the optical counterpart to a gravitational wave source. *Science* 10.1126/science.aap9811 (2017). doi:10.1126/science.aap9811

25. W. L. Freedman, B. F. Madore, B. K. Gibson, L. Ferrarese, D. D. Kelson, S. Sakai, J. R. Mould, R. C. Kennicutt Jr., H. C. Ford, J. A. Graham, J. P. Huchra, S. M. G. Hughes, G. D. Illingworth, L. M. Macri, P. B. Stetson, Final results from the *Hubble Space Telescope* Key Project to measure the Hubble constant. *Astrophys. J.* **553**, 47–72 (2001). doi:10.1086/320638

26. M. R. Drout *et al*., *Science* 10.1126/science.aaq0049 (2017). 10.1126/science.aaq0049

27. Drout et al., *GRB Coordinates Network* 21547 (2017).

28. Materials and methods are available as supplementary materials.

29. Z. Cano, S.-Q. Wang, Z.-G. Dai, X.-F. Wu, The observer's guide to the gamma-ray burst supernova connection. *Adv. Astron.* **2017**, 8929054 (2017). doi:10.1155/2017/8929054

30. E. M. Levesque, J. S. Bloom, N. R. Butler, D. A. Perley, S. B. Cenko, J. X. Prochaska, L. J. Kewley, A. Bunker, H.-W. Chen, R. Chornock, A. V. Filippenko, K. Glazebrook, S. Lopez, J. Masiero, M. Modjaz, A. Morgan, D. Poznanski, GRB 090426: The environment of a rest-frame 0.35-s gamma-ray burst at a redshift of 2.609. *Mon. Not. R. Astron. Soc.* **401**, 963–972 (2010). doi:10.1111/j.1365-2966.2009.15733.x

31. N. R. Tanvir, *et al., GRB Coordinates Network Circular Service* 11123 (2010).

32. A. Cucchiara, J. X. Prochaska, D. Perley, S. B. Cenko, J. Werk, A. Cardwell, J. Turner, Y. Cao, J. S. Bloom, B. E. Cobb, Gemini spectroscopy of the short-hard gamma-ray burst GRB 130603B afterglow and host galaxy. *Astrophys. J.* **777**, 94 (2013). doi:10.1088/0004-637X/777/2/94

33. A. de Ugarte Postigo, C. C. Thöne, A. Rowlinson, R. García-Benito, A. J. Levan, J. Gorosabel, P. Goldoni, S. Schulze, T. Zafar, K. Wiersema, R. Sánchez-Ramírez, A. Melandri, P. D'Avanzo, S. Oates, V. D'Elia, M. De Pasquale, T. Krühler, A. J. van der Horst, D. Xu, D. Watson, S. Piranomonte, S. D. Vergani, B. Milvang-Jensen, L. Kaper, D. Malesani, J. P. U. Fynbo, Z. Cano, S. Covino, H. Flores, S. Greiss, F. Hammer, O. E. Hartoog, S. Hellmich, C. Heuser, J. Hjorth, P. Jakobsson, S. Mottola, M. Sparre, J. Sollerman, G. Tagliaferri, N. R. Tanvir, M. Vestergaard, R. A. M. J. Wijers, Spectroscopy of the short-hard GRB 130603B. *Astron. Astrophys.* **563**, A62 (2014). doi:10.1051/0004-6361/201322985

34. C. D. Kilpatrick, R. J. Foley, D. Kasen, A. Murguia-Berthier, E. Ramirez-Ruiz, D. A. Coulter, M. R. Drout, A. L. Piro, B. J. Shappee, K. Boutsia, C. Contreras, F. Di Mille, B. F. Madore, N. Morrell, Y.-C. Pan, J. X. Prochaska, A. Rest, C. Rojas-Bravo, M. R. Siebert, J. D. Simon, N. Ulloa, Electromagnetic evidence that SSS17a is the result of a binary neutron star merger. 10.1126/science.aaq0073 (2017). doi:10.1126/science.aaq0073

35. A. Murguia-Berthier *et al*., *Astrophys. J. Lett*. 10.3847/2041-8213/aa91b3 (2017). 10.3847/2041-8213/aa91b3

36. M. R. Drout, R. Chornock, A. M. Soderberg, N. E. Sanders, R. McKinnon, A. Rest, R. J. Foley, D. Milisavljevic, R. Margutti, E. Berger, M. Calkins, W. Fong, S. Gezari, M. E. Huber, E. Kankare, R. P. Kirshner, C. Leibler, R. Lunnan, S. Mattila, G. H. Marion, G. Narayan, A. G. Riess, K. C. Roth, D. Scolnic, S. J. Smartt, J. L. Tonry, W. S. Burgett, K. C. Chambers, K. W. Hodapp, R. Jedicke, N. Kaiser, E. A. Magnier, N. Metcalfe, J. S. Morgan, P. A. Price, C. Waters, Rapidly evolving and luminous transients from Pan-STARRS1. *Astrophys. J.* **794**, 23 (2014). doi:10.1088/0004-637X/794/1/23

37. F. Patat, E. Cappellaro, J. Danziger, P. A. Mazzali, J. Sollerman, T. Augusteijn, J. Brewer, V. Doublier, J. F. Gonzalez, O. Hainaut, C. Lidman, B. Leibundgut, K. Nomoto, T. Nakamura, J. Spyromilio, L. Rizzi, M. Turatto, J. Walsh, T. J. Galama, J. van Paradijs, C. Kouveliotou, P. M. Vreeswijk, F. Frontera, N. Masetti, E. Palazzi, E. Pian, The metamorphosis of SN 1998bw. *Astrophys. J.* **555**, 900–917 (2001). doi:10.1086/321526

38. K. Z. Stanek, T. Matheson, P. M. Garnavich, P. Martini, P. Berlind, N. Caldwell, P. Challis, W. R. Brown, R. Schild, K. Krisciunas, M. L. Calkins, J. C. Lee, N. Hathi, R. A. Jansen, R. Windhorst, L. Echevarria, D. J. Eisenstein, B. Pindor, E. W. Olszewski, P. Harding, S. T. Holland, D. Bersier, Spectroscopic discovery of the supernova 2003dh associated with GRB 030329. *Astrophys. J.* **591**, L17–L20 (2003). doi:10.1086/376976

39. B. D. Metzger, R. Fernández, Red or blue? A potential kilonova imprint of the delay until black hole formation following a neutron star merger. *Mon. Not. R. Astron. Soc.* **441**, 3444–3453 (2014). doi:10.1093/mnras/stu802

40. S. Wanajo, Y. Sekiguchi, N. Nishimura, K. Kiuchi, K. Kyutoku, M. Shibata, Production of all the *r*-process nuclides in the dynamical ejecta of neutron star mergers. *Astrophys. J.* **789**, L39 (2014). doi:10.1088/2041-8205/789/2/L39

41. D. Kasen *et al*., *Nature* 10.1038/nature24453 (2017). 10.1038/nature24453

42. P. E. Nugent, M. Sullivan, S. B. Cenko, R. C. Thomas, D. Kasen, D. A. Howell, D. Bersier, J. S. Bloom, S. R. Kulkarni, M. T. Kandrashoff, A. V. Filippenko, J. M. Silverman, G.

W. Marcy, A. W. Howard, H. T. Isaacson, K. Maguire, N. Suzuki, J. E. Tarlton, Y.-C. Pan, L. Bildsten, B. J. Fulton, J. T. Parrent, D. Sand, P. Podsiadlowski, F. B. Bianco, B. Dilday, M. L. Graham, J. Lyman, P. James, M. M. Kasliwal, N. M. Law, R. M. Quimby, I. M. Hook, E. S. Walker, P. Mazzali, E. Pian, E. O. Ofek, A. Gal-Yam, D. Poznanski, Supernova SN 2011fe from an exploding carbon-oxygen white dwarf star. *Nature* **480**, 344–347 (2011). doi:10.1038/nature10644 Medline

43. B. J. Shappee, A. L. Piro, T. W.-S. Holoien, J. L. Prieto, C. Contreras, K. Itagaki, C. R. Burns, C. S. Kochanek, K. Z. Stanek, E. Alper, U. Basu, J. F. Beacom, D. Bersier, J. Brimacombe, E. Conseil, A. B. Danilet, S. Dong, E. Falco, D. Grupe, E. Y. Hsiao, S. Kiyota, N. Morrell, J. Nicolas, M. M. Phillips, G. Pojmanski, G. Simonian, M. Stritzinger, D. M. Szczygieł, F. Taddia, T. A. Thompson, J. Thorstensen, M. R. Wagner, P. R. Woźniak, The young and bright type ia supernova ASASSN-14lp: Discovery, early-time observations, first-light time, distance to NGC 4666, and progenitor constraints. *Astrophys. J.* **826**, 144 (2016). doi:10.3847/0004-637X/826/2/144

44. R. M. Quimby, J. C. Wheeler, P. Hoflich, C. W. Akerlof, P. J. Brown, E. S. Rykoff, SN 2006bp: Probing the shock breakout of a Type II-P supernova. *Astrophys. J.* **666**, 1093–1107 (2007). doi:10.1086/520532

45. R. Pereira, R. C. Thomas, G. Aldering, P. Antilogus, C. Baltay, S. Benitez-Herrera, S. Bongard, C. Buton, A. Canto, F. Cellier-Holzem, J. Chen, M. Childress, N. Chotard, Y. Copin, H. K. Fakhouri, M. Fink, D. Fouchez, E. Gangler, J. Guy, W. Hillebrandt, E. Y. Hsiao, M. Kerschhaggl, M. Kowalski, M. Kromer, J. Nordin, P. Nugent, K. Paech, R. Pain, E. Pécontal, S. Perlmutter, D. Rabinowitz, M. Rigault, K. Runge, C. Saunders, G. Smadja, C. Tao, S. Taubenberger, A. Tilquin, C. Wu, Spectrophotometric time series of SN 2011fe from the Nearby Supernova Factory. *Astron. Astrophys.* **554**, A27 (2013). doi:10.1051/0004-6361/201221008

46. M. R. Drout, A. M. Soderberg, P. A. Mazzali, J. T. Parrent, R. Margutti, D. Milisavljevic, N. E. Sanders, R. Chornock, R. J. Foley, R. P. Kirshner, A. V. Filippenko, W. Li, P. J. Brown, S. B. Cenko, S. Chakraborti, P. Challis, A. Friedman, M. Ganeshalingam, M. Hicken, C. Jensen, M. Modjaz, H. B. Perets, J. M. Silverman, D. S. Wong, The fast and furious decay of the peculiar Type Ic supernova 2005ek. *Astrophys. J.* **774**, 58 (2013). doi:10.1088/0004-637X/774/1/58

47. IRAF is distributed by the National Optical Astronomy Observatory, which is operated by the Association of Universities for Research in Astronomy (AURA) under a cooperative agreement with the National Science Foundation.

48. T. Matheson, R. P. Kirshner, P. Challis, S. Jha, P. M. Garnavich, P. Berlind, M. L. Calkins, S. Blondin, Z. Balog, A. E. Bragg, N. Caldwell, K. D. Concannon, E. E. Falco, G. J. M. Graves, J. P. Huchra, J. Kuraszkiewicz, J. A. Mader, A. Mahdavi, M. Phelps, K. Rines, I. Song, B. J. Wilkes, Optical spectroscopy of Type Ia supernovae. *Astron. J.* **135**, 1598–1615 (2008). doi:10.1088/0004-6256/135/4/1598

49. Flux calibration, www.cfa.harvard.edu/supernova/SNfast/fluxcal.html.

50. J. L. Marshall *et al*., in *Ground-based and Airborne Instrumentation for Astronomy II*, I. S. McLean, M. M. Casali, Eds. (Proceedings of SPIE, 2008), vol. 7014, p. 701454.

51. G. D. Becker, M. Rauch, W. L. W. Sargent, High-redshift metals. I. The decline of C IV at $z>5.3$. *Astrophys. J.* **698**, 1010–1019 (2009). doi:10.1088/0004-637X/698/2/1010

52. R. J. Foley, P. J. Challis, A. V. Filippenko, M. Ganeshalingam, W. Landsman, W. Li, G. H. Marion, J. M. Silverman, R. L. Beaton, V. N. Bennert, S. B. Cenko, M. Childress, P. Guhathakurta, L. Jiang, J. S. Kalirai, R. P. Kirshner, A. Stockton, E. J. Tollerud, J. Vinkó, J. C. Wheeler, J.-H. Woo, Very early ultraviolet and optical observations of the Type Ia supernova 2009ig. *Astrophys. J.* **744**, 38 (2012). doi:10.1088/0004-637X/744/1/38

53. A. Dressler, T. Hare, B. C. Bigelow, D. J. Osip, in *Ground-based and Airborne Instrumentation for Astronomy II*, I. S. McLean, M. Iye, Eds. (Proceedings of SPIE, 2006), vol. 6269, p. 62690F.

54. R. Bernstein, S. A. Shectman, S. M. Gunnels, S. Mochnacki, A. E. Athey, in *Instrument Design and Performance for Optical/Infrared Ground-based Telescopes*, M. Iye, A. F. M. Moorwood, Eds. (Proceedings of SPIE, 2003), vol. 4841, pp. 1694–1704.

55. D. D. Kelson, Optimal techniques in two-dimensional spectroscopy: Background subtraction for the 21st century. *Publ. Astron. Soc. Pac.* **115**, 688–699 (2003). doi:10.1086/375502

56. E. F. Schlafly, D. P. Finkbeiner, Measuring reddening with Sloan Digital Sky Survey stellar spectra and recalibrating SFD. *Astrophys. J.* **737**, 103 (2011). doi:10.1088/0004-637X/737/2/103

57. G. M. Green, E. F. Schlafly, D. P. Finkbeiner, H.-W. Rix, N. Martin, W. Burgett, P. W. Draper, H. Flewelling, K. Hodapp, N. Kaiser, R. P. Kudritzki, E. Magnier, N. Metcalfe, P. Price, J. Tonry, R. Wainscoat, A three-dimensional map of milky way dust. *Astrophys. J.* **810**, 25 (2015). doi:10.1088/0004-637X/810/1/25

58. M. M. Phillips, J. D. Simon, N. Morrell, C. R. Burns, N. L. J. Cox, R. J. Foley, A. I. Karakas, F. Patat, A. Sternberg, R. E. Williams, A. Gal-Yam, E. Y. Hsiao, D. C. Leonard, S. E. Persson, M. Stritzinger, I. B. Thompson, A. Campillay, C. Contreras, G. Folatelli, W. L. Freedman, M. Hamuy, M. Roth, G. A. Shields, N. B. Suntzeff, L. Chomiuk, I. I. Ivans, B. F. Madore, B. E. Penprase, D. Perley, G. Pignata, G. Preston, A. M. Soderberg, On the source of the dust extinction in Type Ia supernovae and the discovery of anomalously strong Na I absorption. *Astrophys. J.* **779**, 38 (2013). doi:10.1088/0004-637X/779/1/38

59. J. A. Cardelli, G. C. Clayton, J. S. Mathis, The relationship between infrared, optical, and ultraviolet extinction. *Astrophys. J.* **345**, 245 (1989). doi:10.1086/167900

60. Y.-C. Pan *et al*., *Astrophys. J.* (2017). 10.3847/2041-8213/aa9116

61. E. Pian *et al*., *Nature* 10.1038/nature24298 (2017). 10.1038/nature24298

62. A. Frebel, N. Christlieb, J. E. Norris, W. Aoki, M. Asplund, The oxygen abundance of HE 1327-2326. *Astrophys. J.* **638**, L17–L20 (2006). doi:10.1086/500592

63. R. Fernández, F. Foucart, D. Kasen, J. Lippuner, D. Desai, L. F. Roberts, Dynamics, nucleosynthesis, and kilonova signature of black hole—neutron star merger ejecta. *Class. Quantum Gravity* **34**, 154001 (2017). doi:10.1088/1361-6382/aa7a77